ISSN 0021-3640, JETP Letters, 2009, Vol. 89, No. 2, pp. 58–62. © Pleiades Publishing, Ltd., 2009.
Original Russian Text © O.A. Aktsipetrov, V.O. Bessonov, A.A. Fedyanin, V.O. Val'dner, 2009, published in Pis'ma v Zhurnal Éksperimental'noĭ i Teoreticheskoĭ Fiziki, 2009, Vol. 89, No. 2, pp. 64–69.

DC-Induced Generation of the Reflected Second Harmonic in Silicon

O. A. Aktsipetrov[a], V. O. Bessonov[a], A. A. Fedyanin[a], and V. O. Val'dner[b]

[a] *Faculty of Physics, Moscow State University, Moscow, 119992 Russia*
e-mail: aktsip@shg.ru
[b] *Moscow State Institute of Radio Engineering, Electronics, and Automation (Technical University), pr. Vernadskogo 78, Moscow, 119454 Russia*

Received December 10, 2008

DC-induced generation of the reflected second harmonic is experimentally observed on the surface of a centrosymmetric silicon single crystal. A direct current with a surface density of $j_{max} \sim 10^3$ A/cm^2 violates the symmetry of the electron distribution function and induces the optical second harmonic with an intensity corresponding to the dipole quadratic susceptibility $\chi^{(2)d}(j_{max}) \sim 3 \times 10^{-15}$ m/V.

PACS numbers: 7.57.Lm, 76.60.-k

DOI: 10.1134/S0021364009020027

The surface nonlinear optics of centrosymmetric media is a rapidly developing line in diagnostic nonlinear optics. Reflected-second-harmonic (SG) generation highly sensitive to surface parameters is used as a convenient tool for studying solid surfaces and solid-state nanostructures [1]. The SG generation induced by external effects plays an important role in these studies. The electrically- and magnetically-induced second harmonics (ESG [2] and MSG [3], respectively) are widely used at present to analyze the electronic and magnetic parameters of surfaces and nanostructures.

The optical and nonlinear-optical parameters of silicon are well known, and this material can be used as a model object for nonlinear-optical studies of centrosymmetric semiconductors. The feature of such materials is that the even-order bulk dipole nonlinear susceptibility tensors are zero; i.e., bulk dipole second-harmonic generation is absent in these materials [4]. The second harmonic in a bulk centrosymmetric medium is determined by the small quadrupole component of the dielectric susceptibility and can be phenomenologically described by the nonlinear polarization vector $\mathbf{P}_{2\omega}^{\text{bulk}} \propto \hat{\chi}^{(2)q,b}\mathbf{E}_\omega\nabla\mathbf{E}_\omega$, where the tensor $\hat{\chi}^{(2)q,b}$ describes the quadrupole quadratic susceptibility of the medium due to the spatial dispersion of the optical pump wave at the frequency ω: $\mathbf{E}_\omega = \mathbf{E}_0\exp(i\omega t - i(\mathbf{kr}))$, where $\mathbf{E}_0$ and $\mathbf{k}$ are the amplitude and wave vector, respectively.

However, violation of the inversion symmetry in the surface layer results in the large dipole contribution to the quadratic nonlinear susceptibility in the presence of a surface. Three mechanisms of inversion-symmetry violation in the surface layer of a centrosymmetric material are pointed out:

(i) Inversion-symmetry violation due to the violation ("break") of the crystallographic-lattice translational symmetry in the surface layer across the surface [5]. The corresponding contribution to the nonlinear polarization of the medium is written as $\mathbf{P}_{2\omega}^{\text{surf}} \propto \hat{\chi}^{(2)d,s}\mathbf{E}_\omega\mathbf{E}_\omega$, where the tensor $\hat{\chi}^{(2)d,s}$ describes the surface dipole quadratic susceptibility;

(ii) Inversion-symmetry violation by an electric field perpendicular to the surface in the space-charge region [6]. The corresponding nonlinear polarization has the form $\mathbf{P}_{2\omega}^{\text{efish}} \propto \hat{\chi}^{(3)d,b}(E^{dc})\mathbf{E}_\omega\mathbf{E}_\omega\mathbf{E}^{\text{dc}}$, where the tensor $\hat{\chi}^{(3)d,b}(E^{\text{dc}})$ describes the bulk dipole cubic susceptibility of the medium, which does not vanish in centrosymmetric media, and $\mathbf{E}^{\text{dc}}$ is the static electric field in the space-charge region;

(iii) Inversion-symmetry violation due to nonuniform surface mechanical deformations of the surface layer [7]. The corresponding contribution to nonlinear polarization is $\mathbf{P}_{2\omega}^{\text{stress}} \propto \hat{\chi}^{(2)d,s}(\sigma)\mathbf{E}_\omega\mathbf{E}_\omega$, where the tensor $\hat{\chi}^{(2)d,s}(\sigma)$ describes the dipole quadratic susceptibility dependent on the stress tensor $\hat{\sigma}$.

In addition to these three mechanisms of inversion-symmetry violation, which are due to noncentrosymmetric deformations of the crystallographic structure of the lattice cell, there exists a mechanism that has not yet been studied experimentally. An electric current through a centrosymmetric semiconductor distorts the equilibrium electron distribution function, which is

symmetric in the quasimomentum space. Hence, a direct current violates the central symmetry of the electronic subsystem. As a result, the nonlinear polarization becomes nonzero: $\mathbf{P}_{2\omega}^{\text{current}}(\mathbf{j}) = \hat{\chi}^{(2)d}(\mathbf{j})\mathbf{E}_{\omega}\mathbf{E}_{\omega}$, where $\mathbf{j}$ is the current density and $\hat{\chi}^{(2)d}(\mathbf{j})$ is the tensor of dipole quadratic susceptibility induced by the direct current with the density $\mathbf{j}$. A microscopic model of current-induced second-harmonic generation in a model direct-band semiconductor was considered in [8]. The density-matrix calculations showed that the asymmetry of the electron distribution function in the conduction band leads to the appearance of the current-induced component $\hat{\chi}^{(2)d}(\mathbf{j})$ in the quadratic susceptibility. The current-induced component has narrow resonance corresponding to the interband electronic transition to the proximity of the Fermi level, is proportional to the current density, $\hat{\chi}^{(2)d}(\mathbf{j}) \propto |\mathbf{j}|$, and changes sign under current reversal: $\hat{\chi}^{(2)d}(\mathbf{j}) = -\hat{\chi}^{(2)d}(-\mathbf{j})$.

The symmetry analysis of silicon (001) single crystals shows that two experimental geometries can be separated for an *s*-polarized pump wave and an *s*-polarized second-harmonic wave (the so-called *s*–*s* combination of the polarizations of the nonlinear interaction). The effect of current-induced second harmonic generation is maximal for the longitudinal (allowed) geometry of the current, where the pump polarization is parallel to the current density. The effect of current-induced second harmonic generation should be absent for the transverse (forbidden) geometry of the current, where the pump polarization is perpendicular to the current density.

In this work, we observe current-induced second harmonic generation due to inversion-symmetry violation by a direct current parallel to the surface.

Figure 1a shows the geometry of the experiment for the detection of the current-induced second harmonic.

Current-induced second harmonic generation was observed in a heavily-doped *p*-Si (001) single crystal with the acceptor number density $N_a = 5 \times 10^{19}$ cm^{-3}. Nickel electrodes 300 ± 30 nm in thickness were deposited onto a silicon surface coated by the natural-oxide film under a residual pressure of 10^{-5} Torr. The gap between the electrodes is aligned with the *X* crystallographic axis, and its width is 200 ± 20 μm. Then, this structure was annealed according to the procedure described in [9] to form the ohmic contact between the silicon and nickel. The resistance of the resulting metal–semiconductor contact is ~0.02 Ω. The directly measured sample temperature in the course of the above experiment was not higher than 40°C. The current density in the surface layer with a thickness of about 50 nm corresponding to the penetration depth for the second harmonic at the wavelength $\lambda_{2\omega} = 390$ nm was $j_{\max} \simeq 10^3$ A/cm^2.

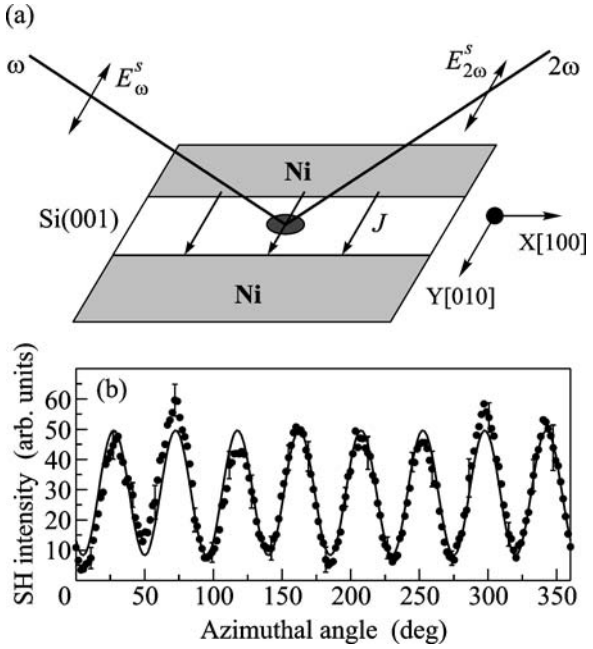

Fig. 1. (a) The scheme of the Si structure with nickel electrodes and details of the nonlinear optics experiment. Here, E^s_ω and $E^s_{2\omega}$ are the *s*-polarized pump wave and second harmonic fields, respectively, and $\mathbf{j}$ is the current density. The reference frame corresponds to the directions of the crystallographic axes. (b) The azimuthal anisotropic dependence of the second harmonic intensity in the *s*–*s* combination of the pump wave and second harmonic polarizations.

A femtosecond Ti:Sap laser with a tunable wavelength in the 700–840-nm range, a pulse duration of 80 fs, a pulse repetition frequency of 86 MHz, and a mean power of 130 mW was the pump radiation source. The radiation incident at an angle of 45° was focused on the electrode gap into a spot of 40-μm diameter. The second harmonic radiation was separated by BG-39 filters with a total thickness of 8 mm and was detected by a photomultiplier operated in the photon-count modes.

Note that the experimental scheme proposed for detecting current-induced second harmonic generation is not free of spurious effects capable of masking true current-induced second harmonic generation attributed to the violation of the symmetry of the electron distribution function. Such spurious effects associated with the direct current effect on second harmonic generation in silicon can be (a) the Joule heating of silicon and temperature variations in optical susceptibilities, (b) the appearance of electrically induced second harmonic component due to the tangential electric field generated by applying a voltage to the current electrodes, and (c) the effect of the current on the second harmonic induced by mechanical stresses.

To eliminate the last spurious effect, the *s*–*s* combination of the pump wave and second harmonic polarizations was used in all our experiments. In this case, only the anisotropic quadrupole second harmonic is

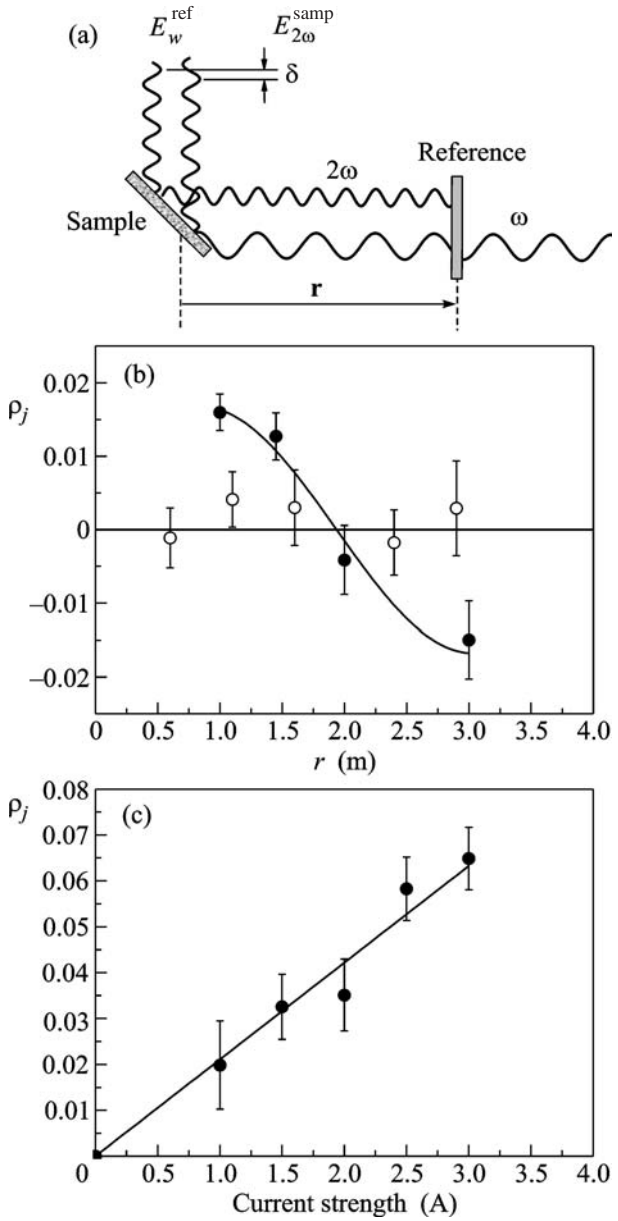

Fig. 2. (a) The scheme of single-path interference of the second harmonic. (b) The interference dependence of the current contrast at a pump wavelength of 780 nm for (closed circles) allowed geometry at the current $J = 1$ A and (open circles) forbidden geometry at the current $J = 4$ A. (c) The current dependence of the current contrast. The pump wavelength is 780 nm.

generated in the (001) bulk silicon [5]. The second harmonic intensity is an oscillating function of the azimuth angle with eight minima and maxima on a noise pedestal (Fig. 1b). If the plane of pump incidence is parallel to the *X* or *Y* silicon crystallographic axes or makes an angle of 45° with these axes, contribution (c) to the second harmonic intensity vanishes. This means that the second harmonic intensity from both the surface and bulk of (001) silicon, including the second harmonic induced by mechanical stresses, vanishes for such geometry.

Discrimination of the masking thermal effects [effects (a) in our above classification] is particularly important. Since the current-induced quadratic susceptibility changes sign under current reversal, the phase of the current-induced second harmonic should be sensitive to the current direction, whereas the thermal effect should be independent of the current orientation. For this reason, we studied current-induced second harmonic generation by the single-path interferometry of the second harmonic [10] with an external second harmonic (reference) source [11] (see Fig. 2a). A 30-nm-thick tin oxide film on a glass substrate was used as a reference. The total intensity $I_{2\omega}(j, r) \sim (\mathbf{E}_{2\omega}^{sample}(j, r) + \mathbf{E}_{2\omega}^{ref}(r))^2$ of the sample and reference second harmonic fields, where $\mathbf{E}_{2\omega}^{sample}(j, r)$ and $\mathbf{E}_{2\omega}^{ref}(r)$ are the complex amplitudes of the sample and reference second harmonic fields, respectively, includes a cross term whose sign changes under current reversal and is a harmonic function of the coordinate r of the sample relative to the reference. Hence, the current-induced second harmonic can be characterized by the so-called current contrast of the second harmonic intensity defined as

$$\rho_j = \frac{I_{2\omega}^{+}(j, r) - I_{2\omega}^{-}(j, r)}{I_{2\omega}^{ref}} \propto 4E_{2\omega}^{ref}E_{2\omega}^{samp}(j)\cos[\delta], \quad (1)$$

where $I_{2\omega}^{+}(j, r)$ and $I_{2\omega}^{-}(j, r)$ are the second harmonic intensities induced by opposite currents and $E_{2\omega}^{samp}(j)$ and $E_{2\omega}^{ref}$ are the corresponding real amplitudes of the sample and reference second harmonics. The phase difference between the second harmonic waves is $\delta = 2\pi r/L + \Phi^{ref} + \Phi^{samp}$, where r is the distance from the reference to the sample, Φ^{samp} and Φ^{ref} are the second harmonic phases, and $L = \lambda_\omega(2\Delta n)^{-1}$ is the interference pattern period, where $\Delta n = n(2\omega) - n(\omega)$.

Thus, all experiments were carried out (i) using second harmonic interferometry with an external reference source to eliminate spurious thermal effects and (ii) in the *ss* combination of the pump and second harmonic polarizations and with the azimuthal orientation of the sample at a crystallographic signal minimum to eliminate the spurious effect of the current on the mechanical stresses and on the bulk quadrupole contribution to the second harmonic intensity. The latter condition was fulfilled automatically for the allowed and forbidden geometries of the current. Each experimental point was obtained by measuring the signals for opposite currents and calculating the current contrast ρ_j.

The closed circles in Fig. 2b correspond to the experimental dependence of the current contrast on the distance between the reference and sample in the case of the allowed geometry of current-induced second har-

monic generation. The solid line is the fit by the oscillating part of Eq. (1) with $L = 4.8$ cm, which corresponds to the air dispersion $\Delta n = n(2\omega) - n(\omega)$ for a pump wavelength of 780 nm [12]. The presence of an interference pattern and the nonzero current contrast is indicative of the sensitivity of the current-induced second harmonic phase to the current direction, i.e., of current-induced second harmonic generation. The reference position maximizing the current contrast was determined using the interference pattern. The further experiments were carried out for this position of the reference. The open circles in Fig. 2b indicate the absence of the current-induced second harmonic generation in the forbidden geometry of the current: the current contrast is zero within the experimental error. Figure 2c shows that the current contrast is a linear function of the current density j. According to Eq. (1), $\rho_j \propto E_{2\omega}^{\text{samp}}(\mathbf{j}) \propto \hat{\chi}^{(2)d}(\mathbf{j})$. Therefore, the linear dependence for ρ_j implies the linear dependence of the current-induced quadratic susceptibility $\hat{\chi}^{(2)d}(\mathbf{j})$ on the current density j in accordance with the theoretical predictions in [8].

There exists another spurious effect that can mask the current-induced second harmonic. If the current is parallel to the surface, then, in addition to the current-induced second harmonic, there can be another second harmonic component due to the tangential electric field E_{driv} generated by the current in the gap. This component can be observed as an electric-induced second harmonic with the same symmetry as the current-induced second harmonic.

However, the following two experimental facts confirm the pure current-induced origin of the observed second harmonic.

First, the spectrum of the electric-induced second harmonic in (001) silicon was studied in [13]. It was shown that the intensity maximum of the electric-induced second harmonic is reached for a second harmonic photon energy of 3.35 eV. The spectrum of the current-induced second harmonic measured in the present work shows that the spectral profiles of the electric- and current-induced second harmonics are significantly different. This implies that the observed effect is not electric induced.

Figure 3a presents the spectral profiles of the current contrast measured in this experiment and the normalized coefficient of the electrically-induced second harmonic from [13]. Note that a peak at about 3.35 eV corresponding to the bulk two-photon resonance of direct transitions in silicon is absent in the current-contrast spectrum. Hence, the observed effect is neither crystallographic nor electrically induced. The existence of a narrow resonance at an energy of about 3.53 eV agrees qualitatively with the results of the theoretical model [8] for current-induced second harmonic generation in semiconductors. The band structure of silicon near the critical point E_0' for the direct transitions is shown in

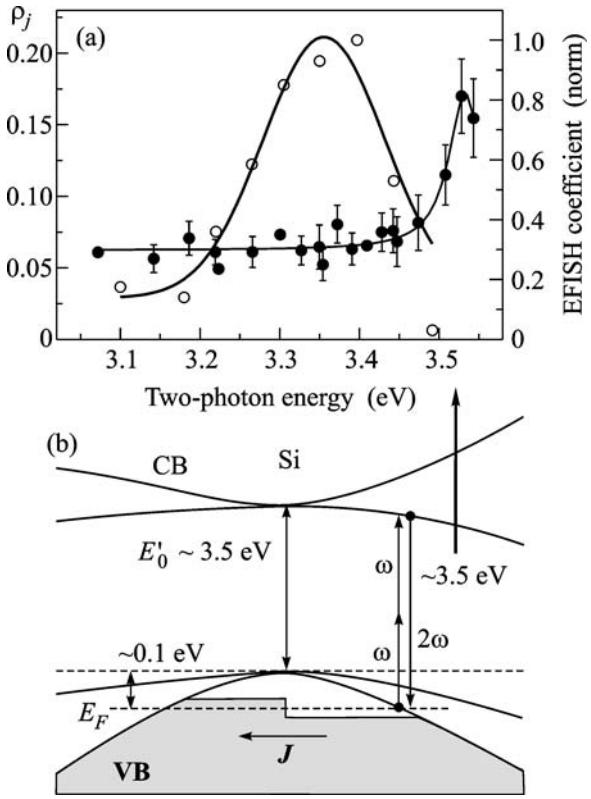

Fig. 3. (a) Spectral profile of the (closed circles) current contrast measured for the current $J = 4$ A and (open circles) electrically-induced second harmonic from [13]. The solid curves are the Lorentz fits of the line. (b) Band structure of heavily doped p-silicon. The electric current J distorts the electron distribution function. This is schematically shown as a step in the valence band. The arrows show the electronic transitions in which pump and second harmonic photons are absorbed or emitted.

Fig. 3b. The hole distribution function for p-type Si is similar to the electron distribution functions considered in model calculations [8]. The local Fermi level at room temperature for heavily-doped p-type Si used in our experiment is in the conduction band and, according to the estimate, is ~0.1 eV below its upper edge for $k = 0$. Therefore, the expected narrow resonance near 3.5 eV is observed in the experiment.

Another piece of evidence in favor of the current, rather than field-effect, nature of the observed effect is provided by the comparison of the expected intensity $I_{2\omega}(E_{\text{driv}})$ for the electric fields used in our experiments and the experimentally measured second harmonic intensity $I_{2\omega}(j)$. Such a comparison shows that the latter intensity is at least two orders of magnitude higher. The interelectrode electric field typical of our samples and experimental conditions is $E_{\text{driv}} \approx 1$ V/cm. At the same time, the typical electric field in the experiments on observations of the electrically-induced second harmonic is $E^{\text{dc}} \approx 10^5$ V/cm [13]. Since the intensity of the electrically-induced second harmonic in such an electrostatic field under the experimental conditions

reported in [13] is about the intensity of the crystallographic *p*-polarized second harmonic from a (001) silicon surface, the intensity $I_{2\omega}(E^{dc})$ can be estimated by the intensity of the reflected *p*-polarized second harmonic measured for our samples. Hence, the ratio $I_{2\omega}(j)/I_{2\omega}(E_{SCR}) \sim 5 \times 10^{-6}$ for the intensity derived using the current contrast ρ_j. This ratio for the second harmonic intensity $I_{2\omega}(E_{driv})$ expected for our experiment is $I_{2\omega}(E_{driv})/I_{2\omega}(E_{SCR}) \propto [E_{driv}/E_{SCR}]^2 \sim 10^{-8}$–$10^{-10}$, which is two orders of magnitude lower than the value for the observed intensity of the current-induced second harmonic.

The comparison of the intensities of the current-induced second harmonic and the second harmonic reflected from the crystalline quartz whose dipole quadratic susceptibility is well known [14] makes it possible to estimate the maximum current-induced quadratic susceptibility in our case: $\chi^{(2)d}(j_{max}) \sim 3 \times 10^{-15}$ m /V.

In conclusion, the results of this work are summarized as follows. Current-induced second harmonic generation in a centrosymmetric silicon single crystal has been experimentally observed. The optical second harmonic corresponding to the dipole quadratic susceptibility $\chi^{(2)d}(j_{max}) \sim 3 \times 10^{-15}$ m/V is induced by a direct current with the surface density $j_{max} \sim 10^3$ A/cm^2. The experimentally observed current-induced effect opens new prospects for the development of novel techniques to measure the direction and density of currents in surface regions of semiconductor devices.

This work was supported by the Russian Foundation for Basic Research (project nos. 06-02-39013 and 07-02-92113).

REFERENCES

1. Y. R. Shen, Nature (London) **337**, 519 (1989).
2. S. H. Lee, R. K. Chang, and N. Bloembergen, Phys. Rev. Lett. **18**, 167 (1967).
3. Ru-Pin Pan, H. D. Wei, and Y. R. Shen, Phys. Rev. B **39**, 1229 (1989).
4. Y. R. Shen, *The Principles of Nonlinear Optics* (Wiley, New York, 1984).
5. H. W. K. Tom, T. F. Heinz, and Y. R. Shen, Phys. Rev. Lett. **51**, 1983 (1983).
6. J. I. Dadap, X. F. Hu, M. H. Anderson, et al., Phys. Rev. B **53**, 7607R (1996).
7. W. Daum, H.-J. Krause, U. Reichel, and H. Ibach, Phys. Rev. Lett. **71**, 1234 (1993).
8. J. B. Hurgin, Appl. Phys. Lett. **67**, 1113 (1995).
9. A. Singh and W. S. Khokle, Proc. of the IEEE **75**, 852 (1987).
10. G. Berkovic, Y. R. Shen, G. Marowsky, and R. Steinhoff, J. Opt. Soc. Am. B **6**, 205 (1989).
11. J. I. Dadap, J. Shan, A. S. Weling, et al., Opt. Lett. **24**, 1059 (1999).
12. O. A. Aktsipetrov, E. D. Mishina, T. V. Misuryaev, et al., Surf. Sci. **402–404**, 576 (1998).
13. O. A. Aktsipetrov et al. Phys. Rev. B **60**, 8924 (1999).
14. *Handbook of Lasers with Selected Data on Optical Technology*, Ed. by R. J. Pressley (Chemical Rubber Co., Cleveland, 1971).

Translated by A. Serber